



Structural mapping of the Goulfey-Tourba (West and Central African Rift) sedimentary basin using high-resolution gravity data

Paul Gautier Kamto^{1,2,*}, Erdinc Oksum³, Willy Lemotio^{1,2}, Joseph Kamguia^{1,2}

1. Geodesy Research Laboratory, National Institute of Cartography (NIC), P.O. Box 157, Yaoundé, Cameroon

2. Department of Physics, University of Yaoundé I, P.O. Box 812, Yaoundé, Cameroon

3. Department of Geophysical Engineering, Süleyman Demirel University, Isparta, Turkey

oksum@istanbul.edu.tr

ABSTRACT

The Goulfey-Tourba sedimentary basin (GTSB) is a portion of the West and Central African Rift System whose studies on its structural geology remain very limited. Belonging to the vast semi-arid Sahelian region, this sedimentary basin covers several localities in Cameroon and Chad, whose economic and social activities are highly impacted by the shortage of drinking water. In this work, a new look is taken at the geological features of this local sedimentary region. To perform this, a preliminary synthetic study is carried out to assess the performance of some classic and recent edge detection methods. The effectiveness of the recent Improved Logistic (IL) method is approved, given its ability to highlight low amplitude and deep features with a refined resolution. A regional/residual separation was applied to Bouguer gravity disturbances to avoid blurring some upper crustal structures by high-frequency anomalies. The effectiveness of this regional/residual separation has been validated by checking the absence of ringing artifacts (Gibbs phenomenon). The application of the IL method on residual gravimetric disturbances of the study area revealed a series of lineaments not yet identified by previous scientific studies. The results show a slight fracturing of the basement, with geological features mainly trending in an NW-SE direction. A newly identified geological discontinuity continuously crosses the study area from 12°45'N latitude to the southeast. Utilizing a modified and recent form of the Euler deconvolution theory (Improved Tilt-Euler method) has enabled the detection of several density sources in the GTSB, most of which correlate well with the lineaments outlined by the IL method. The improved Tilt-Euler method results show anomalous sources at more than 6 km depth beneath the Bodélé sedimentary series of the Upper Tertiary. The Euler's linear solutions attributed to basement fractures show an average depth of 1 km. These results are undoubtedly a major contribution to refining the research of hydrogeological resources in this Sahelian area.

Keywords: Geological features; Improved Logistic method; Improved Tilt-Euler method; Hydrogeological resources; Goulfey-Tourba sedimentary basin.

Mapeo estructural de la cuenca sedimentaria de Goulfey-Tourba (Rift de África Occidental y Central) a través de información de gravedad de alta resolución

RESUMEN

La cuenca sedimentaria de Goulfey-Tourba se encuentra en el sistema de rift de África Central y Occidental, pero sus estudios de geología estructural son muy limitados a la fecha. Perteneciente a la vasta región semiárida del Sahel, esta cuenca sedimentaria cubre varias localidades en Camerún y Chad, cuyas actividades económicas y sociales se ven fuertemente impactadas por la escasez de agua potable. En este trabajo se ofrece una nueva mirada a las características geológicas de esta región sedimentaria. Para el cumplimiento de este objetivo se realizó un estudio sintético preliminar con el fin de medir el desempeño de algunos métodos clásicos y recientes de detección de bordes. Se aprobó la efectividad del reciente método de Logística Mejorada debido a su capacidad para resaltar las amplitudes bajas y las características profundas con una solución fina. Luego se aplicó una separación regional/residual a las anomalías gravitatorias de Bouguer para evitar el desenfoque de algunas estructuras de la corteza superior por las anomalías de alta frecuencia. La efectividad de esta separación regional/residual se ha validado al verificar la ausencia de discontinuidades (fenómeno de Gibbs). La aplicación del método de Logística Mejorada en las anomalías gravimétricas residuales en el área de estudio reveló una serie de lineamientos que no habían sido identificados. Los resultados muestran un fracturamiento ligero en los cimientos, con características geológicas con una tendencia mayoritaria en la dirección NW-SE. Una recién descubierta discontinuidad geológica cruza regularmente el área de estudio desde la latitud 12°45'N hacia el sudeste. Al utilizar una forma recientemente modificada de la teoría de deconvolución de Euler (Método Tilt-Euler mejorado) fue posible detectar varias fuentes de densidad en la cuenca sedimentaria de Goulfey-Tourba, muchas de las cuales están bien correlacionadas con los lineamientos referenciados con el método de Logística Mejorada. Los resultados del método Tilt-Euler mejorado muestran fuentes anómalas a una profundidad de 6 kilómetros debajo de la serie sedimentaria de Bodélé, del Terciario Superior. Las soluciones lineales de Eulers asignadas a las fracturas de los cimientos muestran una profundidad promedio de 1 km. Estos resultados son, sin duda, una contribución mayor en el mejoramiento de la búsqueda de recursos hidrogeológicos en el área del Sahel.

Palabras clave: características geológicas; método de Logística Mejorada; método Tilt-Euler mejorado; recursos hidrogeológicos; cuenca sedimentaria de Goulfey-Tourba.

Manuscript received: 24/04/2023

Accepted for publication: 27/09/2023

How to cite item:

Kamto, P. G., Oksum, E., Lemotio, W., & Kamguia, J. (2023). Structural mapping of the Goulfey-Tourba (West and Central African Rift) sedimentary basin using high-resolution gravity data. *Earth Sciences Research Journal*, 239-249. <https://doi.org/10.15446/esrj.v27n3.108506>

Introduction

The Goulfey-Tourba sedimentary basin (GTSB) is located in the Far North region of Cameroon. Also called Makari Basin, the GTSB constitutes the northern part of the Logone Birni sedimentary basin (LBB) in the Central and West African Rift System (WCRAS) (Loule and Pospisil, 2013). The GTSB also belongs to the large endorheic Chad basin domain. Located between longitudes 14°15' E and 15°15' E, and latitudes 12°12' N and 13°12' N, the GTSB constitutes the main geological formation in the study area (Figure 1). The study area shows a relatively flat topography. Although several localities in this area have been identified as abounding a good hydrogeological potential (Isiorho et al., 1991), few geophysical studies have been carried out to improve the exploitation of groundwater resources. Also, the hydrocarbon potential of the neighboring sedimentary basins, all of them belonging to the WCRAS, makes the GTSB an area of interest for the scientific community (Poudjom et al., 1996; Loule et Pospisil, 2013; Nguimbous-Kouoh et al., 2017). Unfortunately, the available ground-based gravity data are already aged and very sparse to conduct a detailed structural study of the local basin. So, the geophysical investigation of the GTSB requires the use of new high-resolution data and advanced potential field processing methods.

Until today, the Far North region of Cameroon in general and especially the GTSB, is still suffering from great difficulties in accessing potable drinking water (Fantong et al., 2010; Cheo et al., 2017). This water shortage considerably affects the economic development of the region and population health. According to Lianchong et al. (2011) and Hasan et al. (2019), the identification of faults and underground geological formations is a major asset for the exploitation of groundwater contained in the underlying aquifers. A precise mapping of the fractured-rock aquifers in the region would be an undeniable contribution to the project of installation of water boreholes in the most affected localities. Besides, the optimal exploitation of hydrocarbons and mineral resources available to the region is a necessity to ensure sustainable development. This requires a preliminary geometric characterization of underground anomalies (Wang and Huang, 2012; Ugbor et al., 2021; Habu et al., 2022). The precision provided in the delineation of geological structures depends on the method and the quality of the data used (Ammar and Kamal, 2018; Hasan et al., 2019; Ekwok et al., 2020; Deep et al., 2021).

The use of the gravimetric method for the characterization of structural features in the basement has been successfully applied in hydrogeophysics according to recent scientific projects (Redhaouia et al., 2016; Epuh, 2020; Taha et al., 2021; Ziani et al., 2022). The improvement and optimization of data acquisition techniques during the latest satellite missions enable the production of global gravity field models with unprecedented resolution and accuracy (Andersen et al., 2020; Guo et al., 2020; Müller and Wu, 2020; Gautier et al., 2022). On the other hand, the detection techniques of geological lineaments are widely and increasingly used in structural geophysics (Kamto et al., 2021; Pham et al., 2021; Eldosouky et al., 2021, 2022a; Ekwok et al., 2021; al., 2022; Ekka et al., 2022; Kamto et al., 2023a). For decades, new edge detection methods have been developed by researchers to provide better results in the mapping of structural features, and to avoid the occurrence of extraneous noise which could be assigned to geological features (Wijns et al., 2005; Cooper and Cowan, 2006; Tatchum et al., 2011; Oksum et al. (2021); Pham, 2021; Melouah and Pham, 2021; Pham et al., 2022; Prasad et al., 2022). Most of these processing methods are designed using vertical or horizontal derivatives of amplitude, basically used to highlight sharp gradient areas in a potential field. The classic horizontal gradient (Cordell and Grauch, 1985) and total gradient (Roest et al., 1992) filters are among the most widely used techniques in structural geophysics. Based on these latter and mathematical functions, Wijns et al. (2005), Ferreira et al. (2013) and Pham et al. (2020) proposed some edge detection methods mainly based on the ratio of derivatives of the gradient of the amplitude; these methods are respectively the theta map, the tilt angle of the total horizontal gradient and the improved logistic filter. Since then, these advanced and new techniques are commonly exploited to produce quality results in structural geology and tectonics (Ekka et al., 2022; Eldosouky et al., 2022b; Ekwok et al., 2022; Ghomsi et al., 2022; Kafadar, 2022; Sahoo et al., 2022; Arogundade et al., 2023).

This work aims to achieve a precise and detailed structural mapping of the GTSB using a high-resolution global gravity model XGM2019e (Zingerle et al., 2020). In order to evaluate their performance, the horizontal gradient (THG),

the total gradient (TG), the theta map (TM), the tilt angle of the total horizontal gradient (TTHG) and the improved logistic (IL) techniques are beforehand tested through a complex synthetic model. Then, to delineate lineaments and faults of the GTSB, these techniques are applied to the topography-free gravity disturbances. Additionally, the Euler deconvolution method (Thompson, 1982 and Reid et al., 1990) is used to estimate the depth of anomalous discontinuities in the basement.

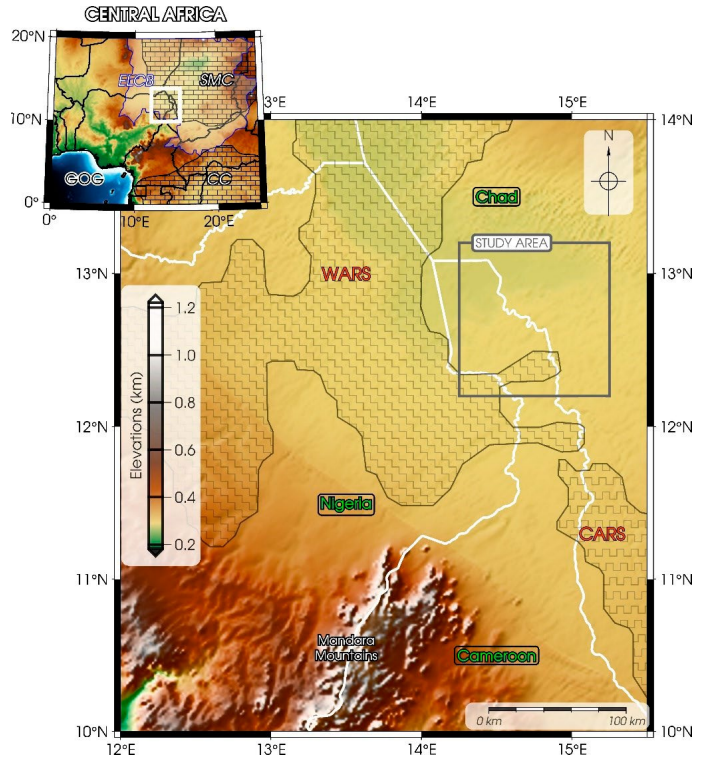


Figure 1. Location and topographic map of the Goulfey-Tourba sedimentary basin in the Far North region of Cameroon. The region's main geological structures are the West African Rift System (WARS) and the Central African Rift System (CARS). White lines represent national boundaries. The inset exhibits Central Africa and some geological and tectonic units including the Endorheic Lake Chad Basin (ELCB), the Sahara MetaCraton (SMC) and the Congo Craton (CC). The white box circumscribes the Far North region of Cameroon and its surroundings. GOG: Gulf of Guinea.

2. Geologic and tectonic framework

Figure 2a shows a simplified view of the major geological formations and structures in Central Africa. The GTSB belongs to one of the largest geological structures of the African lithospheric plate, namely the WCARS. The tectonic evolution of Central Africa is strongly linked to its major geological units, especially the Congo craton and the Sahara metacraton, the Cameroon line, the WARS and CARS (Moreau et al., 1987; Fairhead, 1988; Binks and Fairhead, 1992). The young deposits of the Cenozoic era are the main geological formation of the CARS and thus, of the GTSB. Guiraud et al. (1992) affirmed that the evolution of the CARS between Nigeria, Cameroon and Chad during the break-up of Gondwana would be at the origin of the appearance of strong stresses between tectonic plates, inducing the reactivation of tectonic structures in the study area. The geological patterns of the GTSB are presented in Figure 2b and is linked to the formation of the endorheic Lake Chad basin during the Cretaceous period. There are four main geological formations in the area, namely: the Bodele serie (dating of Pliocene times), the Soulias serie (from the upper Pleistocene), the Labde serie (from the upper Holocene) and volcanic rocks (Mathieu, 1976). These geological formations cover granitic and gneissic rocks in the basement. Loule and Pospisil (2013) showed that the GTSB is the site of volcanic bodies dating from the Cretaceous and trapped in the crustal

basement. According to these authors, the geological stresses caused by the extension and uplift of the Mesozoic LBB would be the main cause of tectonic structures, and thus, of the underlying magmatic intrusions.

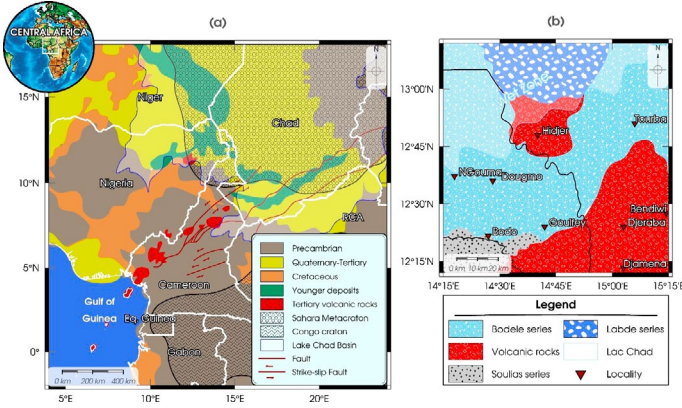


Figure 2. (a) Simplified view of major geological formations and structures in Central Africa. (b) Geological patterns of the Goulfey-Tourba sedimentary basin (Modified from Nguimbous-Kouoh et al., 2017).

Data and Method

Gravity disturbances

To access structural and geological information at a local scale such as the study area, the exploitation of high-resolution and accurate data is essential. In this work, the global gravity model XGM2019e has been utilized. It is one of the most recent gravity models improved following a series of anterior global models namely XGM2016 (Pail et al., 2018), XGM2019 and XGM2019e_2159 (Zingerle et al., 2020). The gravity field model XGM2019e has been developed using satellite altimetry data, terrestrial and marine gravity data, gravity effects of topography and the satellite gravity model GOCO06s. This high-resolution global gravity field model contains spherical harmonic coefficients up to degree and order (d/o) 5399 (~2° or 4 km of spatial resolution). The gravity data derived from satellite altimetry and topography has been computed respectively from the 1°x1° spatial resolution DTU13 (Andersen et al., 2016) and EARTH2014 (Hirt and Rexer, 2015) models. The combination of satellite data with terrestrial data has been made using normal equation complete derivation for spectral bands up to d/o 719, and the use of a block diagonal least squares regression technique for d/o above 719 (Zingerle et al., 2020). By performing some comparison tests with GPS/levelling points, Zingerle et al. (2020) showed a slight improvement in the XGM2019e gravity model on land compared to its predecessors (EGM2008, XGM2016 and EIGEN6C4). This global gravity model is increasingly exploited and validated in many recent studies in geodynamics and structural geophysics (Abrehdary and Sjoberg, 2021; Samprieto and Capponi, 2021; Ognev et al., 2022; Lewerissa and Laponi, 2023; Li et al., 2023).

Gradient-based filters

Edge enhancement techniques in structural geology and geophysics have experienced a particular boom since the end of the 20th century. One of the most classic and widely used methods is the horizontal gradient mathematically formulated in its completed form for the first time by Cordell (1979). The HG method is established from the variations of the potential field along the x and y directions. Representing a field of gravimetric disturbances $A(x,y)$ as a regular grid of points (i,j) with amplitudes $A_{i,j}$, an approximation of its first order derivatives in the x and y directions can be written as follows:

$$D_x = \frac{\partial A}{\partial x} \approx \frac{A_{i+1,j} - A_{i-1,j}}{2|x_{i+1} - x_i|} \quad (1)$$

and,

$$D_y = \frac{\partial A}{\partial y} \approx \frac{A_{i,j+1} - A_{i,j-1}}{2|y_{i+1} - y_i|} \quad (2)$$

So, the HG is defined as the amplitude generated by the D_x and D_y components:

$$HG(x, y) = (D_x^2 + D_y^2)^{1/2} \quad (3)$$

Besides, Nabighian (1972) introduced the analytical signal method on a three-dimensional potential field. Also called the total gradient method, the analytical signal was discovered as a technique for outlining structural features according to the study of Roest et al. (1992). This method is defined as follows:

$$TG(x, y) = (D_x^2 + D_y^2 + D_z^2)^{1/2} \quad (4)$$

Unlike the HG, the TG integrates three components of the potential field: D_x , D_y , and the first-order vertical derivative D_z . It was Evjen (1936) who first introduced this notion and its importance in the interpretation of gravity anomalies. The vertical gradient can be easily calculated in the frequency domain using the fast Fourier transform F and the radial repetency k of the potential field (Gunn, 1975):

$$D_z = \frac{\partial A}{\partial z} \approx F^{-1} [|k| F(A)] \quad (5)$$

Phase-based filters

In order to overcome the limitations of gradient filters, many researchers introduced a wide variety of phase-based edge detection methods. The THETA method, proposed by Wijns et al. (2005), is basically an improvement of the TG method in the delineation of magnetic anomalous sources at low latitudes. Therefore, this method has been undervalued for almost two decades for the gravimetric processing of geological features (Oruc, 2011; Kumar et al., 2022). The THETA filter is defined as the phase difference between HG and TG functions. So, this filter could be expressed as follows:

$$THETA = \cos^{-1} \left(\frac{HG}{TG} \right) \quad (6)$$

Like the THETA method, the TTHG method (Ferreira et al., 2013) is a phase-based filter developed to balance both deep and shallow amplitudes of the potential field. It is an improvement of the tilt angle method (Miller and Singh, 1994) which integrates as the main variable. So, this method is designed by normalizing the vertical derivative of by its horizontal gradient:

$$TTHG = \tan^{-1} \left[\frac{HG_z}{(HG_x^2 + HG_y^2)^{1/2}} \right] \quad (7)$$

where HG_x , HG_y and HG_z are respectively the first-order derivatives of HG in the x-, y- and z-directions.

Improved logistic method

Beyond the numerous edge detection methods in the scientific literature (mainly derivative- and phase-based filters), Pham et al. (2020) recently designed the IL method to increase the precision and resolution of the outlined geological lineaments. This method associates the improved logistic function and the total horizontal gradient. The IL method is defined as follows:

$$IL = \frac{1}{1 + \left[-p \left(\left(\frac{HG_z}{(HG_x^2 + HG_y^2)^{1/2}} \right) - 1 \right) + 1 \right]} \quad (8)$$

The parameter p in Ep. (8) is a positive real constant and its value has a great influence on the resolution of results. An estimation of the optimal p -value has been discussed by Pham et al. (2020) (values between 2 and 5 leading to best resolutions). In this work, the IL method is applied for $p = 2$. Although its performance has already been confirmed by many recent geophysical studies (Ekka et al., 2022; Eldosouky et al., 2022b; Ekwok et al., 2022; Kafadar, 2022; Sahoo et al., 2022; Arogundade et al., 2023), the advantages and limitations of the IL method will first be evaluated on a synthetic model before its application in the study area.

Improved Tilt-Euler deconvolution

The first version of the Euler deconvolution method, widely used in estimating the depths of crustal anomalous sources, was introduced by Thompson (1982) and subsequently adapted in its 3D form by Reid et al. (1990). The main problem with this classic Euler deconvolution theory is that it incorporates a parameter called Structural Index (SI), which the choice greatly influences the precision and quality of the estimated solutions. Several authors have already proposed modified forms of the Euler deconvolution formula to minimize the influence of the SI parameter. One of the modified forms is the Tilt-Euler deconvolution (Salem et al., 2008) which has the advantage of remove the SI parameter as input value. To further improve the previous form which is limited to points where the horizontal gradient of the potential field is different from zero, Huang et al. (2019) recently proposed another modified form called the Improved Tilt-Euler deconvolution method:

$$(x - x_0) \frac{\partial \theta}{\partial x} + (y - y_0) \frac{\partial \theta}{\partial y} + (z - z_0) \frac{\partial \theta}{\partial z} = 0 \quad (9)$$

where the triplets (x, y, z) and (x_0, y_0, z_0) are respectively the geographical coordinates of the observed anomaly and of the anomalous source to be estimated; θ represents the improved tilt angle given by:

$$\theta = \arctan\left(\frac{D_z}{T_G}\right) \quad (10)$$

4. Test of edge detection methods

The methods for delineating geological discontinuities presented in section 4 represent filters of the potential field which, despite their effectiveness, could show some limitations in certain circumstances. In this section, a complex synthetic model is established to evaluate the efficiency of these filters. Figures 3a and 3b show respectively a layout of synthetic density sources in the plan and in 3D. The proposed model consists of five prismatic sources (A, B, C, D and E) with alternately positive and negative density contrasts, and located at different depths. Another peculiarity in the arrangement of the prismatic sources is that D and E induce a certain asymmetry in the proposed synthetic model. Table 1 summarizes the geometric and density parameters of the five prismatic sources.

Table 1. Geometric and density parameters of prismatic bodies.

Parameters/ Prisms	A	B	C	D	E
Coordinates of the center in km	(50,150)	(100,100)	(150,50)	(150,150)	(150,150)
(x-length, y-length) in km	(80,20)	(80,20)	(80,20)	(50,50)	(30,30)
(Width, depth to top) in km	(4,2)	(4,6)	(4,10)	(5,7)	(5,2)
Density contrast (g/cm ³)	0.2	-0.3	0.3	-0.3	0.2

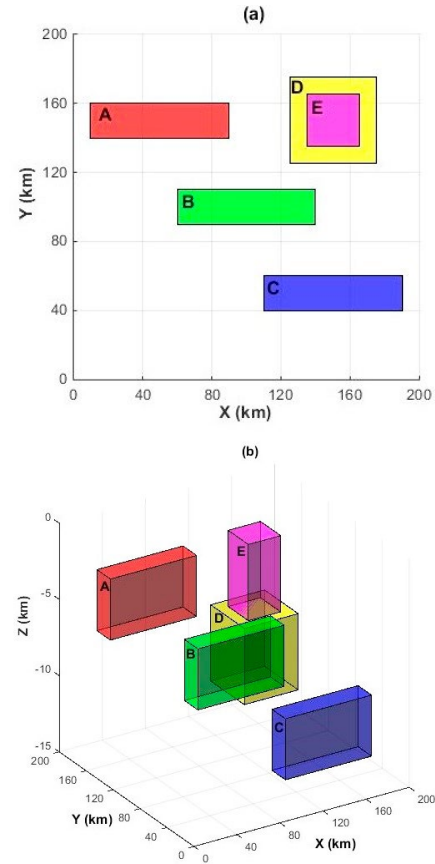


Figure 3. Layout of synthetic bodies in (a) 2D and (b) 3D.

The gravity anomaly model displayed in Figure 4a is generated by the five synthetic bodies (A, B, C, D and E). This model is presented on a grid of dimensions 200 km \times 200 km, with a spatial resolution of 1 km. The results of applying the HG, TG, THETA, TTHG and IL methods to the gravity anomaly are respectively shown in Figures 4b-f. At first glance, the HG classic filter doesn't generate noise or spurious signals around the edges of prismatic bodies. However, the HG filter manages to maximize the signal only on the boundaries of prisms A and E, thus neglecting the existence of other density sources. Unlike the HG method, the TG and THETA methods induce spurious signatures around A, B, C and D. The true boundaries of the density sources are diffused, probably because of the asymmetric arrangement due to D and E prismatic bodies. This assertion is justified by the difficulty of the TG and THETA filters to outline the edges of prism A, although buried at the same depth (2 km) and having the same density contrast (0.2 g/cm³) as prism E. Even in the case of a synthetic model with a symmetric arrangement of density sources, the THETA method already showed some limitations with the appearance of untrue surrounding signatures in the results (Oksum et al., 2021; Pham et al., 2022). Despite spurious signatures produced by the asymmetry in the arrangement of the density sources, the results of the TTHG (Figure 4e) and IL (Figure 4f) methods are more realistic than those presented previously. The amplitudes are well maximized at the boundaries of the five prisms. However, the best resolution goes to the IL filter which refines and maximizes the signatures on the boundaries of the five density sources. Pham et al. (2020) also attested a good accuracy of the IL method on thin prisms compared to the TTHG method.

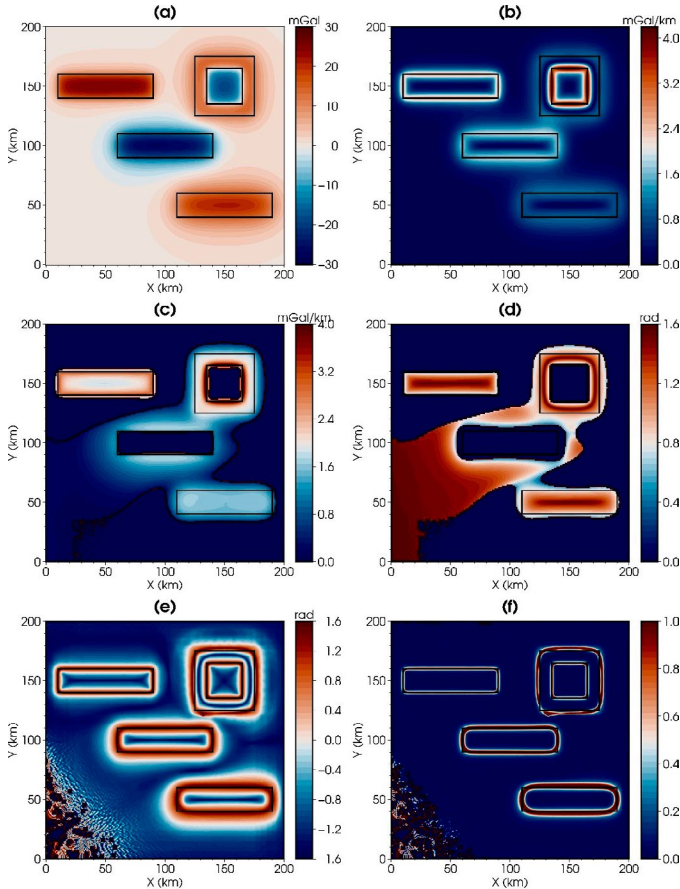


Figure 4. (a) Gravity anomalies generated from the synthetic density sources A, B, C, D, and E, and results from the application of the (b) HG, (c) TG, (d) THETA, (e) TTHG and (f) IL methods on the gravity anomaly grid.

The filters assessed in this section are now performed in a disturbed environment. For this, a white noise of 4% of the amplitude of the synthetic gravity anomalies initially produced has been added to obtain the noisy gravity anomalies (Figure 5a). The results of applying the HG, TG, THETA, TTHG and IL methods to the noisy gravity anomaly are displayed in Figures 5b-f. The result displayed in Figure 5b shows that the HG filter seems less sensitive to the white noise contained in the gravity anomaly grid. In addition, the TG and THETA filters have great difficulties in highlighting the edges of the density sources. The wrong signals generated by the asymmetrical arrangement of bodies D and E are still visible in the southwestern part of Figures 5c and 5d. Unlike the classic HG filter, the TTHG and IL filters accentuate surrounding noise in the displayed results (Figures 5e and 5f). However, the edges of the five prisms A, B, C, D and E are still visible, with better sharpness and less spurious signals in the results following the application of the IL method (Pham et al., 2020).

With the aim of reducing the negative influence of white noise on the results displayed by edge detection filters, the upward continuation filter is commonly required as a solution. So, Figure 6a presents the noisy gravity anomaly upward extended to an elevation of 2 km. Figures 6b-f show the results of applying the HG, TG, THETA, TTHG and IL methods to the gravity anomaly grid of Figure 6a. The spurious signals caused by the white noise injection have considerably disappeared on the HG and TG results. Yet, the precise identification of the edges of prisms A, B, C and D is difficult and limited. The result of the THETA method shows for the first time (contrary to the results of Figures 4d and 5d) a minimization of the amplitude near the edges of the density sources. However, the outlined boundaries are diffused outside the true edges of prisms A, B, C and D (Figure 6d). In spite of the spurious amplitudes which persist as shown in Figures 6a and 6b, the TAHG and IL methods maximize well the amplitudes on the edges of the five prisms. But, the TAHG filter seems to thicken the edges of the prismatic bodies and generate more intrusive signatures compared to the IL filter. So among the five edge detection methods evaluated in this section, the IL method shows the best performance in delineating density source boundaries.

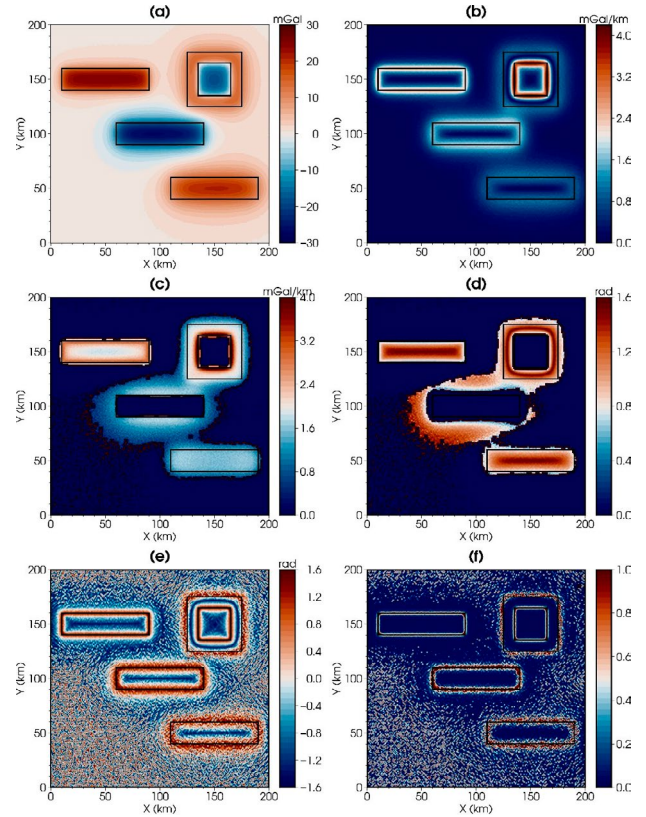


Figure 5. (a) Noisy gravity anomalies generated from the synthetic density sources A, B, C, D, and E, and results from the application of the (b) HG, (c) TG, (d) THETA, (e) TTHG, and (f) IL methods on the noisy gravity anomaly grid.

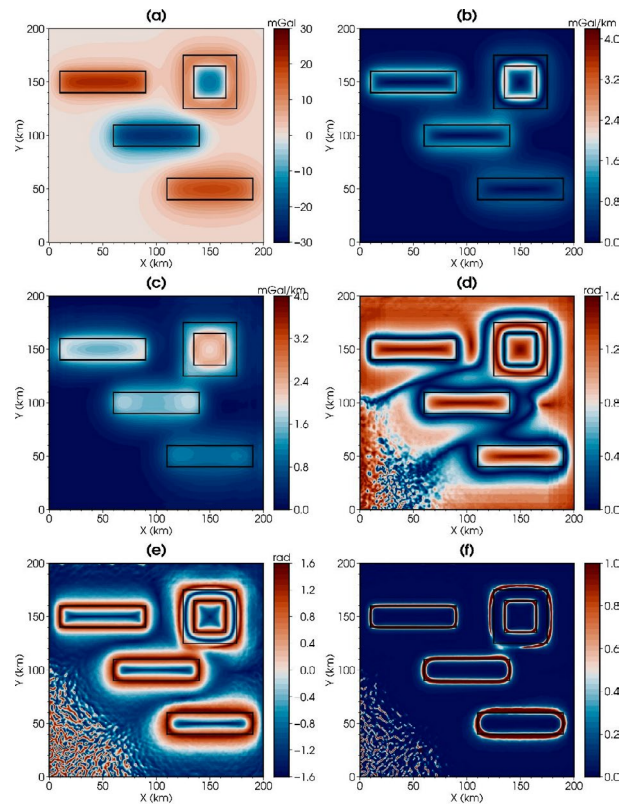


Figure 6. (a) 2 km upward continued noisy gravity anomalies generated from the synthetic density sources A, B, C, D, and E, and results from the application of the (b) HG, (c) TG, (d) THETA, (e) TTHG and (f) IL methods on the noisy gravity anomaly grid.

5. Results and Discussion

Gravity disturbances

The gravity disturbances utilized in the work are derived from the combined gravity field model XGM2019e (Zingerle et al., 2020). The free-air gravity disturbances of the study area are displayed in Figure 7a. This free-air gravity grid has been downloaded with a spatial resolution of 0.033 degree and at a height of 10 km above the ellipsoid to avoid distorting the spectrum of the original gravity field model. The free-air gravity disturbances range from -4.45 to 10.04 mGal, with a mean of 2.23 mGal (Figure 7a). The lowest amplitudes are observed over the young deposits and trend in a N45°E direction. To reveal the gravimetric signatures induced by the major sedimentary formations, and the anomalous crustal and mantle density structures, it is necessary to subtract the gravimetric effects of the topography (Uieda et al., 2016; Kamto et al., 2023b). There are several methods to reduce the topographic effect in the scientific literature (Grombein et al., 2013; De Gaetani et al., 2021). The study area is circumscribed at a very local scale, and the influence of the curvature of the Earth has been neglected. The topographic corrections are calculated using the EARTH2014 global topographic model (Hirt and Rexer, 2015) and at a constant average density of 2670 kg/cm³. Then, we obtain the Topography-free gravity disturbances (Figure 5b), approximated here to the Bouguer gravity disturbances. The amplitudes of Bouguer gravity disturbances in the study area are completely negative and range from -36.78 to -22.88 mGal. The lowest amplitudes correlate approximately with the Bodele geological series (Figure 2b), essentially made up of sediments belonging to the Upper Tertiary (Mathieu, 1976).

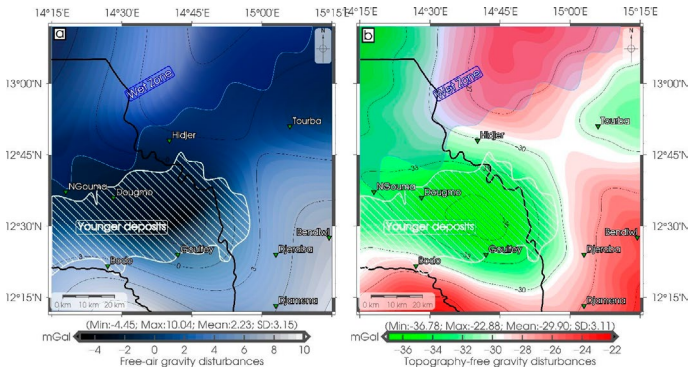


Figure 7. (a) Free-air and (b) Topography-free gravity disturbances in the study area.

Regional/Residual gravity disturbances

For a better delineation of the geological features of the GTSB, it is advantageous to separate the regional gravity disturbances (generally attributed to density anomalies extending from the lower crust to the mantle) from the residual ones. Several regional/residual separation methods exist in the scientific literature (Beltrao et al., 1991; Keating and Pinet, 2011; Mallick and Sharma, 1999; Meng et al., 2009). Each of these methods could be limited and subjective depending on the characteristics of the gravity anomaly grid or the filtering technique used. Kebede et al. (2020) recently conducted a comparative analysis of the most widely used regional/residual separation methods namely the upward continuation (Jacobsen, 1987) and the polynomial trend analysis (Simpson, 1954); they concluded a better reliability of the upward continuation technique provided that the continuation height is suitably estimated. For this study, the spectral analysis (Spector and Grant, 1979) and upward continuation methods have been appropriately applied to the Bouguer gravity disturbance grid (Figure 7b). After an estimation of the continuation height (20 km) using spectral analysis, the grid of regional disturbances is obtained (Figure 8a). The regional disturbances model displays negative amplitudes ranging from -33.47 to -24.74 mGal. These disturbances clearly reflect the regional anomalous trend of the Moho in the study area. The residual disturbances displayed in Figure 7b are obtained by subtracting the regional amplitudes (Figure 8b) from the topography-free gravity disturbances (Figure 7b). The residual

gravity disturbances range from -5.97 to 4.74 mGal; they correlate well with the signatures of the initial gravity disturbances grid and the geological series mainly made up of Tertiary sediments (Figure 8b). Although the signatures observed on the grid of the residual gravity disturbances seem realistic, the authenticity of the latter will be further verified in the results section. Indeed, when applying the regional/residual separation filter, the Gibbs phenomenon (Bocher, 1906) could occur and generate ringing artefacts (spurious signals) in the output model.

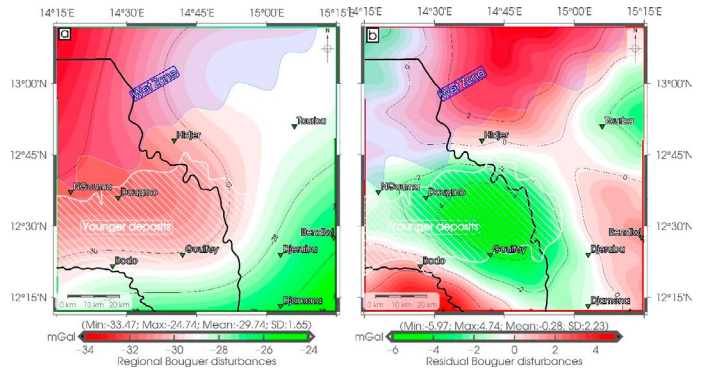


Figure 8. (a) Regional and (b) Residual Bouguer disturbances computed using spectral analysis and upward continuation method.

Application of edge detection filters

Derivatives and Gradient maps

By applying equations 1, 2 and 5 to the amplitudes of the residual gravity disturbances, the x-, y-, and z-derivatives maps are obtained (Figures 9a-c). These derivative maps show the primary contribution of each directional gradient for the characterization of geological structures and formations of the GTSB. The x-derivative (Dx) gives an overview of geological discontinuities or contacts along the x direction. The Dx map vividly shows a majority of geological discontinuities with a NW-SE trend. The y-derivative (Dy) map has a slight similarity with the Dx map in the Southwest, notably a WNW-ESE trending gradient. The z-derivative (Dz) map shows gradient amplitudes ranging from -0.52 to 0.53 mGal. The Dz map amplifies the amplitudes of anomalous density sources and geological transition zones. Some signatures on the Dz map correlate with those displayed on the Dx map.

For a better overview of the geological structures delineated in the study area, the Dx, Dy and Dz components are combined in the classic HG and TG filters. Figures 10a and 10b display the results of applying the HG and TG filters respectively on the residual Bouguer grid of Figure 8b. The HG and TG maps maximize the signal over geological discontinuities, as reported by Cordell (1976) and Roest et al. (1992). The HG map gives very little information on the geological features of the study area. The boundaries of main crustal density sources are difficult to identify. The results displayed by the TG map are not better, despite the addition of the vertical component Dz. As mentioned in the synthetic example in section 4, the delineation of both shallow and deep lineaments by the HG and TG methods remains inaccurate and limited.

THETA and TTHG maps

To solve the main limitations of gradient filters that only highlight high gradient areas (Pham et al., 2020), a series of phase-based methods are introduced to detect both deep and low amplitude of geological structures. Figures 10a and 10b show the results of applying the phase-based THETA and TTHG filters to residual Bouguer disturbances. Unlike the HG and TG maps, the THETA map minimizes the signal (zero amplitude) on geological discontinuities (Wijns et al., 2005). The THETA map seems to delineate more lineaments. But, the outlined lineaments are continuously attached to each other, which does not reflect reality. Ting-Jie et al. (2016) and Oksum et al. (2021) also pointed out the limit of the THETA method mainly because of the wrong signals generated in the result. In addition, the TTHG map (Figure 10b) maximizes the amplitudes of geological features of the GTSB around 1.5 rad (Ferreira et al., 2013). Like the THETA map, the TTHG map depicts the boundaries of geological density

sources with more details, but with the advantage of reducing the appearance of wrong edges in the results. However, as also mentioned by Melouah and Pham (2021), and Oksum et al. (2021), the main disadvantage of the TTHG method

is that it uses to scatter the signal around the true lineaments. A structural study at a local scale such as the study area requires the use of a precise and high-resolution method.

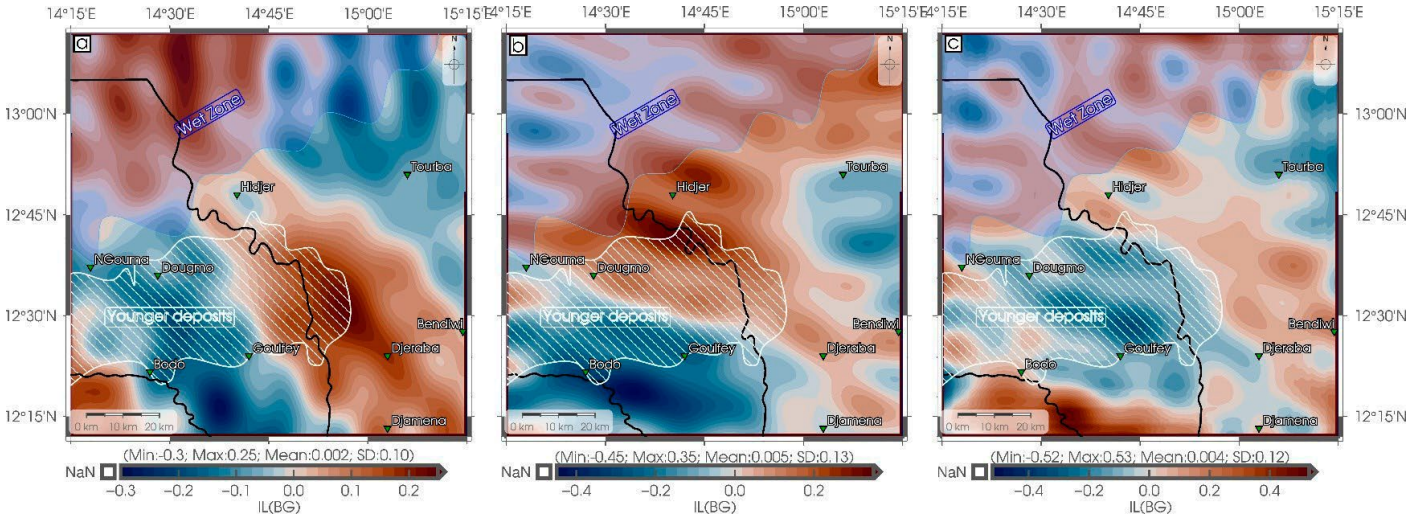


Figure 9. x-derivative (a), y-derivative (b), and z-derivative (c) maps of residual Bouguer disturbances

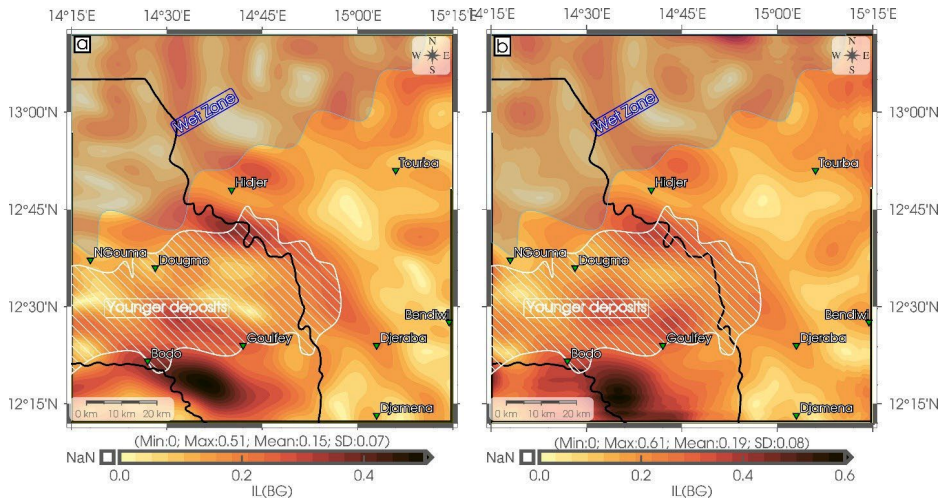


Figure 10. Results of the application of the HG (a) and TG (b) methods on the residual Bouguer disturbances.

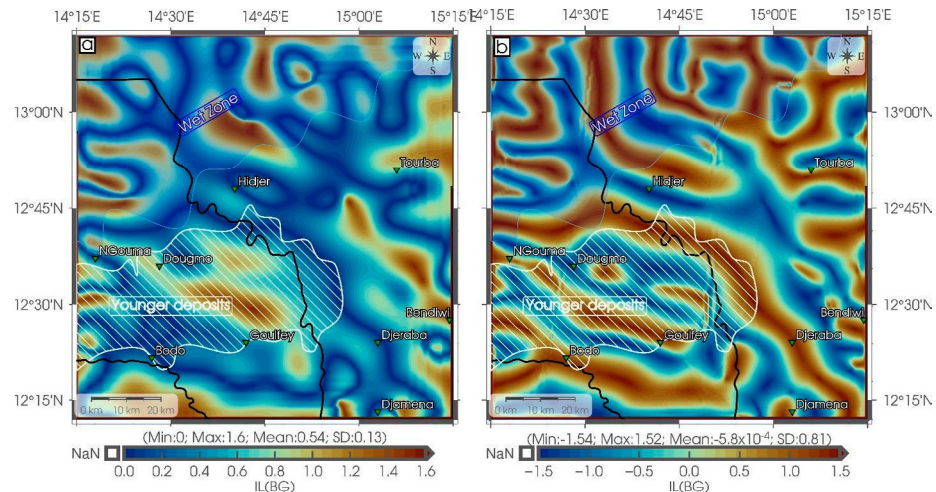


Figure 11. Results of applying the THETA (a) and TTHG (b) methods on the residual Bouguer disturbances.

Application of the IL method

Figure 12a presents the IL method's results to the residual Bouguer disturbances in the study area. The IL map displays maximum amplitudes on geological features and edges of anomalous bodies (Pham et al., 2020). The IL method is also applied to the Bouguer gravity disturbances to verify that the regional/residual separation applied in subsection 5.2 did not produce ringing artifacts in the residual disturbances grid (Figure 7b). The IL(BG) map displays the results of applying the IL method to Bouguer gravity disturbances (Figure 12b). The amplitudes of geological discontinuities outlined in Figure 12a (IL map) show a good correlation with those depicted in Figure 12b (IL(BG) map). The slight differences observed could be mainly caused by the presence of regional amplitudes in the IL(BG) map, which slightly blurs the geological features in some zones. The highlighted features using the IL method are similar to the results displayed on the TTHG map (Figure 11b). However, the display of geological edges on the IL map seems sharper and more precise compared to precedent maps. The effectiveness of the IL method in structural geology has also been confirmed by several recent studies (Eldosouky et al., 2022; Sahoo et al., 2022; Ekka et al., 2022; Maden and Elmas, 2022).

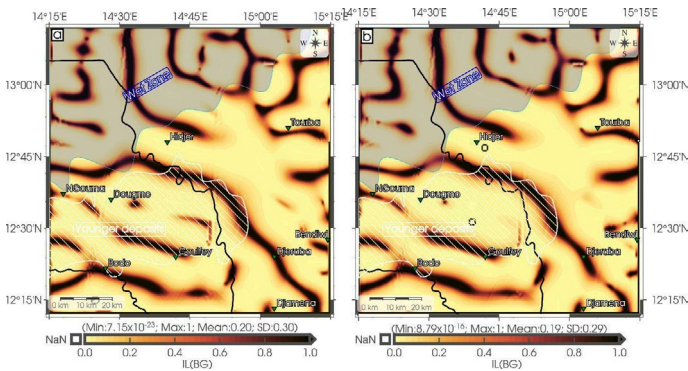


Figure 12. Results of the application of the IL method on (a) the residual Bouguer disturbances and (b) the Bouguer gravity disturbances.

Structural map of the Goulfey-Tourba basin

Following the resolution and precision of the results provided by the IL method, new geological features have been delineated in the basin. Figure 13a shows the geological lineaments identified from the IL method in the GTSB. A total of 28 geological features have been outlined, with lengths ranging from 2.55 to 116.25 km. Figure 13b presents a rose diagram showing the lineament orientation in the study area. Major geological features mainly trending in the NNW-SSE direction are observed. This main direction brings some details to the work of Nguimbous-Kouoh et al. (2017), who rather concluded on NE-SW and NW-SE trending features in the basin. The outlined features can be attributed to fractures, boundaries of intrusive anomalous bodies or contact zones between geological formations. A geological feature newly identified and continuously passing through the study area from latitude 12°45'N up to the Southeast has been enhanced. Never mentioned in previous studies (Loule and Pospisil, 2013; Nguimbous-Kouoh et al., 2017), this geological feature could be attributed to a density contrast between two main geological formations. The work of Guiraud et al. (1982) revealed that the appearance of stress zones between tectonic plates during the opening of the South Atlantic could have reactivated some tectonic features in the basement. The linear features (considered as basement fracturing) observed in Figure 13a denote a slight reactivation of crustal tectonic structures. The fractured areas could greatly help improve the exploration of hydrogeological resources and reduce the problem of lack of drinking water that severely affects the study area (Fantong et al., 2010; Cheo et al., 2017).

Improved Tilt-Euler solutions

Estimating the average depth of anomalous density sources is important in structural geology. One of the classic methods widely used to evaluate the position and the depth of the contours of intrusive bodies is the Euler deconvolution method (Thompson, 1982). In this work, one of its most recent

modified forms is utilized: the improved Tilt-Euler deconvolution method (Huang et al., 2019). This Euler deconvolution form (as defined in equation 9) has the advantage of ignoring the SI parameter as input data. During the computation phase, a compromise has been made for the optimum window size and depth tolerance parameters (respectively 15 and 10%). Too-high values of window size tended to produce spurious solutions around geological discontinuities, while too-low values produced scatters solutions not located on the structural features. Figure 14a displays the solutions proposed by the improved Tilt-Euler deconvolution method in the study area. Most of the Tilt-Euler solutions correlate well with the lineaments delineated by the IL method. In addition, the displayed solutions provide an estimation of the GTSB density sources depths. As depicted in the histogram (Figure 14b), the estimated depths range between 0.27 and 6.27 km, with a mean of 2.09 km. The maximum percentage is attributed to depths estimated between 1 and 1.2 km. The Tilt-Euler solutions confirm the presence of a major discontinuity extending from latitude 12°45'N up to the South-East, as identified on the lineament map (Figure 13.a). The anomalous sources mainly take a NW-SE trend, probably following the tectonic events that the basin underwent during the evolution of the CARS as announced by Guiraud et al. (1992). The location of density sources at more than 4 km depth should induce the scientific community to research potential hydrocarbon resources in this still unexplored sedimentary basin. The linear solutions estimated at 1 km depth on average and coinciding with the structural features of Figure 13a give evidence of a slight fracturing of the basement in the study area. The fractured zones of the basement up to 1 km depth could potentially lead to a water table and should therefore be the target of hydrogeological investigation.

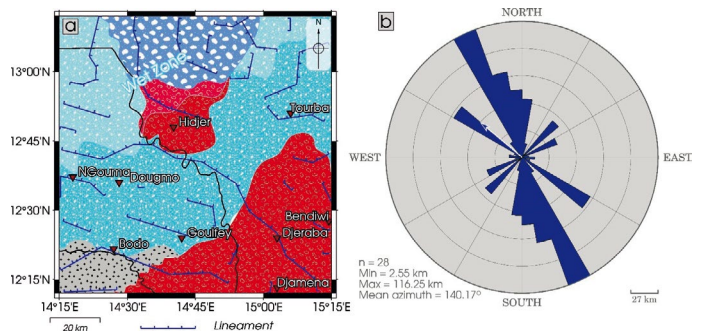


Figure 13. (a) Map of geological lineaments from the IL method; (b) Rose diagram showing lineament orientations in the study area.

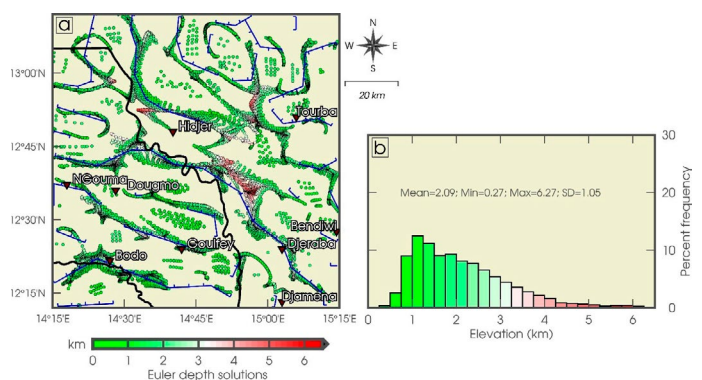


Figure 14. (a) Location and depth of anomalous sources according to the Tilt-Euler deconvolution method; (b) Histogram of frequencies of Tilt-Euler solutions as a function of elevations (depth).

Conclusions

The GTSB covers a local zone in Central Africa and serves as the transition between the WARS and CARS geological structures. The structural geology of this study area remains limited and its hydrogeological potential resources

are still under-exploited given the serious lack of drinking water in the region. This work aimed to reveal new patterns on the structural geology of the GTSB using recent processing methods of potential field. The synthetic assessment of the IL method validates the performance of this latter to delineate with a good precision both shallow and deep geological features. Besides, the classic HG and TG methods have shown great limitations in delineating low gradient amplitude and deep geological features. The application of the IL method on the residual gravity disturbances provides new patterns in the structural geology of the GTSB. The lineaments outlined in the study area mainly trend in a NE-SW direction; this clearly explains the tectonic evolution of the WCARS and its consequences in the reactivation of tectonic structure. However, the structural impact of the tectonic evolution of the area would have been slight given the density of the delineated geological features. A major geological discontinuity, not yet identified by previous studies and continuously passing through the study area from latitude 12°45' N up to the South-East, should contribute for updating the geological map of this area. The application of a recent modified form of the Euler deconvolution method enables to estimate the location and the depths of anomalous density sources (between 0.27 and 6.27 km). The location of linear structures identified as basement fractures and located at an average depth of 1 km, could be potential solutions to refine the hydrogeological investigations in this local region. Besides, the identification of anomalous density sources (with depths estimated at more than 6 km) must be the target of hydrocarbon research in this still unexploited sedimentary basin. However, additional geological and geophysical studies deserve to be carried out in this area, which is arousing scientific interest in recent years.

References

- Abrehdary, M., & Sjöberg, L. E. (2021). A new moho depth model for fennoscandia with special correction for the glacial isostatic effect. *Pure and Applied Geophysics*, 178, 877-888. <https://doi.org/10.1007/s00024-021-02672-8>
- Andersen, O. B., & Knudsen, P. (2020). The DTU17 global marine gravity field: First validation results. *Fiducial Reference Measurements for Altimetry: Proceedings of the International Review Workshop on Satellite Altimetry Cal/Val Activities and Applications* (pp. 83-87). Springer International Publishing.
- Ammar, A. I., & Kamal, K. A. (2018). Resistivity method contribution in determining of fault zone and hydro-geophysical characteristics of carbonate aquifer, eastern desert, Egypt. *Applied water science*, 8, 1-27. <https://doi.org/10.1007/s13201-017-0639-9>
- Andersen, O., Knudsen, P., & Stenseng, L. (2016). The DTU13 MSS (mean sea surface) and MDT (mean dynamic topography) from 20 years of satellite altimetry. In *IGFS 2014: Proceedings of the 3rd International Gravity Field Service (IGFS), Shanghai, China, June 30-July 6, 2014* (pp. 111-121). Springer International Publishing.
- Arogundade, A. B., Ajama, O. D., Ayinde, I. S., Falade, S. C., & Awoyemi, M. O. (2023). Investigation of structural controls on the drainage system of north-western Nigeria. *Acta Geophysica*, 1-16. <https://doi.org/10.1007/s11600-022-01007-y>
- Beltrao, J. F., Silva, J. B. C., & Costa, J. C. (1991). Robust polynomial fitting method for regional gravity estimation. *Geophysics*, 56(1), 80-89. <https://doi.org/10.1190/1.1442960>
- Binks, R. M., & Fairhead, J. D. (1992). A plate tectonic setting for Mesozoic rifts of West and Central Africa. *Tectonophysics*, 213(1-2), 141-151. [https://doi.org/10.1016/0040-1951\(92\)90255-5](https://doi.org/10.1016/0040-1951(92)90255-5)
- Bocher, M. (1906). Introduction to the Theory of Fourier's Series. *The Annals of Mathematics*, 7(3), 81-152. <https://doi.org/10.2307/1967238>
- Cheo, A. E., Voigt, H. J., & Wendland, F. (2017). Modeling groundwater recharge through rainfall in the Far-North region of Cameroon. *Groundwater for sustainable development*, 5, 118-130. <https://doi.org/10.1016/j.gsd.2017.06.001>
- Cooper, G. R. J., & Cowan, D. R. (2006). Enhancing potential field data using filters based on the local phase. *Computers & Geosciences*, 32(10), 1585-1591. <https://doi.org/10.1016/j.cageo.2006.02.016>
- Cordell, L. (1979). Gravimetric expression of graben faulting in Santa Fe country and the Espanola basin, New Mexico. *Guidebook to Santa Fe Country, 30th Field Conference* (pp. 59-64). New Mexico Geological Survey.
- Cordell, L., & Grauch, V. J. S. (1985). Mapping basement magnetization zones from aeromagnetic data in the San Juan Basin, New Mexico. Hinz, W. J. (Ed.) *The utility of regional gravity and magnetic anomaly maps* (pp. 181-197). Society of Exploration Geophysicists. <https://doi.org/10.1190/1.0931830346.ch16>
- De Gaetani, C. I., Marotta, A. M., Barzaghi, R., Reguzzoni, M., & Rossi, L. (2021). The gravity effect of topography: A comparison among three different methods. In: Erol, B., & Erol, S. (Eds.) *Geodetic Sciences-Theory, Applications and Recent Developments* (pp. 1-15). IntechOpen. <https://doi.org/10.5772/intechopen.97718>
- Deep, M. A., Araffa, S. A. S., Mansour, S. A., Taha, A. I., Mohamed, A., & Othman, A. (2021). Geophysics and remote sensing applications for groundwater exploration in fractured basement: A case study from Abha area, Saudi Arabia. *Journal of African Earth Sciences*, 184, 104368. <https://doi.org/10.1016/j.jafrearsci.2021.104368>
- Ekka, M. S., Sahoo, S. D., Pal, S. K., Singha Roy, P. N., & Mishra, O. P. (2022). Comparative analysis of the structural pattern over the Indian Ocean basins using EIGEN6C4 Bouguer gravity data. *Geocarto International*, 1-29. <https://doi.org/10.1080/10106049.2022.2087748>
- Eldosouky, A. M., Pham, L. T., El-Qassas, R. A., Hamimi, Z., & Oksum, E. (2021). Lithospheric structure of the Arabian-Nubian shield using satellite potential field data. In: Hamimi, Z., Fowler, A. R., Liégeois, J. P., Collins, A., Abdelsalam, M. G., & El-Wahed, M. A. (Eds.). *The geology of the Arabian-Nubian shield*, 139-151. https://doi.org/10.1007/978-3-030-72995-0_6
- Eldosouky, A. M., El-Qassas, R. A., Pham, L. T., Abdelrahman, K., Alhumimidi, M. S., El Bahrawy, A., ... & Sehsah, H. (2022a). Mapping main structures and related mineralization of the Arabian Shield (Saudi Arabia) using sharp edge detector of transformed gravity data. *Minerals*, 12(1), 71. <https://doi.org/10.3390/min12010071>
- Eldosouky, A. M., Ekwok, S. E., Akpan, A. E., Achadu, O. I. M., Pham, L. T., Abdelrahman, K., ... & Alarifi, S. S. (2022b). Delineation of structural lineaments of Southeast Nigeria using high resolution aeromagnetic data. *Open Geosciences*, 14(1), 331-340. <https://doi.org/10.1515/geo-2022-0360>
- Ekwok, S. E., Akpan, A. E., Kudamnya, E. A., & Ebong, E. D. (2020). Assessment of groundwater potential using geophysical data: a case study in parts of Cross River State, south-eastern Nigeria. *Applied Water Science*, 10(6), 1-17. <https://doi.org/10.1007/s13201-020-01224-0>
- Ekwok, S. E., Akpan, A. E., Achadu, O. I. M., Thompson, C. E., Eldosouky, A. M., Abdelrahman, K., & Andr  s, P. (2022). Towards understanding the source of brine mineralization in Southeast Nigeria: Evidence from high-resolution airborne magnetic and gravity data. *Minerals*, 12(2), 146. <https://doi.org/10.3390/min12020146>
- Epuh, E. E., Okolie, C. J., Daramola, O. E., Ogunlade, F. S., Oyatayo, F. J., Akinnusi, S. A., & Emmanuel, E. O. I. (2020). An integrated lineament extraction from satellite imagery and gravity anomaly maps for groundwater exploration in the Gongola Basin. *Remote Sensing Applications: Society and Environment*, 20, 100346. <https://doi.org/10.1016/j.rsase.2020.100346>
- Evjen, H. M. (1936). The place of the vertical gradient in gravitational interpretations. *Geophysics*, 1(1), 127-136. <https://doi.org/10.1190/1.1437067>
- Fairhead, J. D. (1988). Mesozoic plate tectonic reconstructions of the central South Atlantic Ocean: the role of the West and Central African rift system. *Tectonophysics*, 155(1-4), 181-191. [https://doi.org/10.1016/0040-1951\(88\)90265-X](https://doi.org/10.1016/0040-1951(88)90265-X)

- Fantong, W. Y., Satake, H., Ayonghe, S. N., Suh, E. C., Adelana, S. M., Fantong, E. B. S., ... & Zhang, J. (2010). Geochemical provenance and spatial distribution of fluoride in groundwater of Mayo Tsanaga River Basin, Far North Region, Cameroon: implications for incidence of fluorosis and optimal consumption dose. *Environmental geochemistry and health*, 32, 147-163. <https://doi.org/10.1007/s10653-009-9271-4>
- Ferreira, F. J., de Souza, J., Bongiolo, A. B. S., & de Castro, L. G. (2013). Enhancement of the total horizontal gradient of magnetic anomalies using the tilt angle. *Geophysics*, 78(3), J33-J41. <https://doi.org/10.1190/geo2011-0441.1>
- Gautier, K. P., Loudi, Y., Alain, Z. A., Ludovic, K. H., Séverin, N., & Joseph, K. (2022). Evaluation of global gravity field models using shipborne free-air gravity anomalies over the Gulf of Guinea, Central Africa. *Survey Review*, 54(384), 243-253. <https://doi.org/10.1080/00396265.2021.1921519>
- Ghomsi, F. E. K., Pham, L. T., Steffen, R., Ribeiro Filho, N., & Tenzer, R. (2022). Delineating structural features of North Cameroon using the EIGEN6C4 high resolution global gravitational model. *Geological Journal*, 57(10), 4285-4299. <https://doi.org/10.1002/gj.4544>
- Grombein, T., Seitz, K., & Heck, B. (2013). Optimized formulas for the gravitational field of a tesseroid. *Journal of Geodesy*, 87, 645-660. <https://doi.org/10.1007/s00190-013-0636-1>
- Guiraud, R., Binks, R. M., Fairhead, J. D., & Wilson, M. (1992). Chronology and geodynamic setting of Cretaceous-Cenozoic rifting in West and Central Africa. *Tectonophysics*, 213(1-2), 227-234. [https://doi.org/10.1016/0040-1951\(92\)90260-D](https://doi.org/10.1016/0040-1951(92)90260-D)
- Gunn, P. J. (1975). Linear transformations of gravity and magnetic fields. *Geophysical prospecting*, 23(2), 300-312. <https://doi.org/10.1111/j.1365-2478.1975.tb01530.x>
- Guo, X., Ditmar, P., Zhao, Q., & Xiao, Y. (2020). Improved recovery of temporal variations of the Earth's gravity field from satellite kinematic orbits using an epoch-difference scheme. *Journal of Geodesy*, 94, 1-16. <https://doi.org/10.1007/s00190-020-01392-6>
- Habu, S. J., Adekeye, O. A., & Tende, A. W. (2022). Structural and geophysical constraint mapping for hydrocarbon resources within parts of the Bida Basin, Central Nigeria. *Arabian Journal of Geosciences*, 15(24), 1760. <https://doi.org/10.1007/s12517-022-11040-2>
- Hasan, M., Shang, Y. J., Jin, W. J., & Akhter, G. (2019). Investigation of fractured rock aquifer in South China using electrical resistivity tomography and self-potential methods. *Journal of Mountain Science*, 16(4), 850-869. <https://doi.org/10.1007/s11629-018-5207-8>
- Heiskanen, W. A., & Moritz, H. (1967). Physical geodesy. *Bulletin Geodesique*, 86, 491-492. <https://doi.org/10.1007/BF02525647>
- Hirt, C., & Rexer, M. (2015). Earth2014: 1 arc-min shape, topography, bedrock and ice-sheet models—available as gridded data and degree-10,800 spherical harmonics. *International Journal of Applied Earth Observation and Geoinformation*, 39, 103-112. <https://doi.org/10.1016/j.jag.2015.03.001>
- Huang, L., Zhang, H., Sekelani, S., & Wu, Z. (2019). An improved Tilt-Euler deconvolution and its application on a Fe-polymetallic deposit. *Ore Geology Reviews*, 114, 103114. <https://doi.org/10.1016/j.oregeorev.2019.103114>
- Isiorho, S. A., Taylor-Wehn, K. S., & Corey, T. W. (1991). Locating groundwater in Chad Basin using remote sensing technique and geophysical method. *EOS (Transactions of the American Geophysical Union)*, 72(44), 220-221.
- Jacobsen, B. H. (1987). A case for upward continuation as a standard separation filter for potential-field maps. *Geophysics*, 52(8), 1138-1148. <https://doi.org/10.1190/1.1442378>
- Kafadar, Ö. (2022). Applications of the Kuwahara and Gaussian filters on potential field data. *Journal of Applied Geophysics*, 198, 104583. <https://doi.org/10.1016/j.jappgeo.2022.104583>
- Kamto, P. G., Lemotio, W., Tokam, A. P. K., & Yap, L. (2021). Combination of terrestrial and satellite gravity data for the characterization of the southwestern coastal region of Cameroon: appraisal for hydrocarbon exploration. *International Journal of Geophysics*, 1-14. <https://doi.org/10.1155/2021/5554528>
- Kamto, P. G., Oksum, E., Luan, T. P., & Kamguia, J. (2023a). Contribution of advanced edge detection filters for the structural mapping of the Douala Sedimentary Basin along the Gulf of Guinea. *Vietnam Journal of Earth Sciences*. <https://doi.org/10.15625/2615-9783/18410>
- Kamto, P. G., Lemotio, W., & Kamguia, J. (2023b). Moho Geometry Estimation Beneath the Gulf of Guinea From Satellite Gravity Data Based on a Regularized Non-Linear Gravity Inversion. *Earth and Space Science*, 10(5). <https://doi.org/10.1029/2023EA002864>
- Keating, P., & Pinet, N. (2011). Use of non-linear filtering for the regional-residual separation of potential field data. *Journal of Applied Geophysics*, 73(4), 315-322. <https://doi.org/10.1016/j.jappgeo.2011.02.002>
- Kebede, H., Alemu, A., & Fisseha, S. (2020). Upward continuation and polynomial trend analysis as a gravity data decomposition, case study at Ziway-Shala basin, central Main Ethiopian rift. *Heliyon*, 6(1), e03292. <https://doi.org/10.1016/j.heliyon.2020.e03292>
- Kumar, U., Narayan, S., & Pal, S. K. (2022). Structural and tectonic interpretation of EGM2008 gravity data around the Laccadive ridge in the Western Indian Ocean: an implication to continental crust. *Geocarto international*, 37(11), 3179-3198. <https://doi.org/10.1080/10106049.2020.1856193>
- Maden, N., & Elmas, A. (2022). Major tectonic features and geodynamic setting of the Black Sea Basin: Evidence from satellite-derived gravity, heat flow, and seismological data. *Tectonophysics*, 824, 229207. <https://doi.org/10.1016/j.tecto.2022.229207>
- Mallick, K., & Sharma, K. K. (1999). A finite element method for computation of the regional gravity anomaly. *Geophysics*, 64(2), 461-469. <https://doi.org/10.1190/1.1444551>
- Mathieu, P. (1976). *Évolution géologique récente du bassin du Tchad*. ORSTOM. Note 12, 12 p.
- Melouah, O., & Pham, L. T. (2021). An improved ILTHG method for edge enhancement of geological structures: application to gravity data from the Oued Righ valley. *Journal of African Earth Sciences*, 177, 104162. <https://doi.org/10.1016/j.jafrearsci.2021.104162>
- Meng, X., Guo, L., Chen, Z., Li, S., & Shi, L. (2009). A method for gravity anomaly separation based on preferential continuation and its application. *Applied Geophysics*, 6(3), 217. <https://doi.org/10.1007/s11770-009-0025-y>
- Miller, H. G., & Singh, V. (1994). Potential field tilt—a new concept for location of potential field sources. *Journal of applied Geophysics*, 32(2-3), 213-217. [https://doi.org/10.1016/0926-9851\(94\)90022-1](https://doi.org/10.1016/0926-9851(94)90022-1)
- Moreau, C., Regnault, J. M., Déruelle, B., & Robineau, B. (1987). A new tectonic model for the Cameroon Line, Central Africa. *Tectonophysics*, 141(4), 317-334. [https://doi.org/10.1016/0040-1951\(87\)90206-X](https://doi.org/10.1016/0040-1951(87)90206-X)
- Müller, J., & Wu, H. (2020). Using quantum optical sensors for determining the Earth's gravity field from space. *Journal of Geodesy*, 94(8), 71. <https://doi.org/10.1007/s00190-020-01401-8>
- Nabighian, M. N. (1972). The analytic signal of two-dimensional magnetic bodies with polygonal cross-section: its properties and use for automated anomaly interpretation. *Geophysics*, 37(3), 507-517. <https://doi.org/10.1190/1.1440276>
- Nguimbous-Kouoh, J. J., Ngos III, S., Mbarga, T. N., & Manguelle-Dicoum, E. (2017). Use of the Polynomial Separation and the Gravity Spectral Analysis to Estimate the Depth of the Northern Logone Birni Sedimentary Basin (CAMEROON). *International Journal of Geosciences*, 8(12), 1442. <https://doi.org/10.4236/ijg.2017.812085>
- Lewerissa, R., & Laponio, L. A. (2023). Identification of sediment-basement structure in West Papua province, Indonesia, using gravity and magnetic data inversion as an Earth's crust stress indicator. *Acta Geophysica*, 71(1), 209-226. <https://doi.org/10.1007/s11600-022-00913-5>

- Li, J., Wu, G., Xu, C., Chen, H., Yan, J., & Zhang, X. (2023). Influence of gravity stripping in the South China Sea area on Moho inversion. *Progress in Geophysics*, 38(1), 31-46. <https://doi.org/10.6038/pg2023GG0083>
- Lianchong, L., Tianhong, Y., Zhengzhao, L., Wancheng, Z., & Chunan, T. (2011). Numerical investigation of groundwater outbursts near faults in underground coal mines. *International Journal of Coal Geology*, 85(3-4), 276-288. <https://doi.org/10.1016/j.coal.2010.12.006>
- Loule, J. P., & Pospisil, L. (2013). Geophysical evidence of Cretaceous volcanics in Logone Birni Basin (northern Cameroon), Central Africa, and consequences for the West and Central African rift system. *Tectonophysics*, 583, 88-100. <https://doi.org/10.1016/j.tecto.2012.10.021>
- Ognev, I., Ebbing, J., & Haas, P. (2022). Crustal structure of the Volgo-Uralian subcraton revealed by inverse and forward gravity modelling. *Solid Earth*, 13(2), 431-448. <https://doi.org/10.5194/se-13-431-2022>
- Oksum, E., Le, D. V., Vu, M. D., Nguyen, T. H. T., & Pham, L. T. (2021). A novel approach based on the fast sigmoid function for interpretation of potential field data. *Bulletin of Geophysics and Oceanography*, 62(3), 543-556. <https://doi.org/10.4430/bgta0348>
- Oruç, B. (2011). Edge detection and depth estimation using a tilt angle map from gravity gradient data of the Kozaklı-Central Anatolia Region, Turkey. *Pure and applied geophysics*, 168(10), 1769-1780. <https://doi.org/10.1007/s00024-010-0211-0>
- Pail, R., Fecher, T., Barnes, D., Factor, J. F., Holmes, S. A., Gruber, T., & Zingerle, P. (2018). Short note: the experimental geopotential model XGM2016. *Journal of geodesy*, 92, 443-451. <https://doi.org/10.1007/s00190-017-1070-6>
- Pham, L. T., Van Vu, T., Le Thi, S., & Trinh, P. T. (2020). Enhancement of potential field source boundaries using an improved logistic filter. *Pure and Applied Geophysics*, 177, 5237-5249. <https://doi.org/10.1007/s00024-020-02542-9>
- Pham, L. T. (2021). A high resolution edge detector for interpreting potential field data: A case study from the Witwatersrand basin, South Africa. *Journal of African Earth Sciences*, 178, 104190. <https://doi.org/10.1016/j.jafrearsci.2021.104190>
- Pham, L. T., Oliveira, S. P., Le, M. H., Trinh, P. T., Vu, T. V., Duong, V. H., ... & Eldosouky, A. M. (2021). Delineation of structural lineaments of the Southwest Sub-basin (East Vietnam Sea) using global marine gravity model from CryoSat-2 and Jason-1 satellites. *Geocarto International*, 1-18. <https://doi.org/10.1080/10106049.2021.1981463>
- Pham, L. T., Eldosouky, A. M., Oksum, E., & Saada, S. A. (2022). A new high resolution filter for source edge detection of potential field data. *Geocarto International*, 37(11), 3051-3068. <https://doi.org/10.1080/10106049.2020.1849414>
- Poudjom, D. Y. H., Legeley-Padovani, A., Boukeke, D. B., Nnange, J. M., Ateba-Bekoa, Y. A., & Fairhead, J. D. (1996). *Levés gravimétriques de reconnaissance-Cameroun*. Orstom, France.
- Prasad, K. D., Pham, L. T., & Singh, A. P. (2022). Structural mapping of potential field sources using BHG filter. *Geocarto International*, 1-28. <https://doi.org/10.1080/10106049.2022.2048903>
- Redhaounia, B., Bédir, M., Gabtni, H., Batobo, O. I., Dhaoui, M., Chabaane, A., & Khomsi, S. (2016). Hydro-geophysical characterization for groundwater resources potential of fractured limestone reservoirs in Amdoun Monts (North-western Tunisia). *Journal of Applied Geophysics*, 128, 150-162. <https://doi.org/10.1016/j.jappgeo.2016.03.005>
- Reid, A. B., Allsop, J. M., Granser, H., Millett, A. T., & Somerton, I. W. (1990). Magnetic interpretation in three dimensions using Euler deconvolution. *Geophysics*, 55(1), 80-91. <https://doi.org/10.1190/1.1442774>
- Roest, W. R., Verhoef, J., & Pilkington, M. (1992). Magnetic interpretation using the 3-D analytic signal. *Geophysics*, 57(1), 116-125. <https://doi.org/10.1190/1.1443174>
- Sahoo, S. D., Narayan, S., & Pal, S. K. (2022). Fractal analysis of lineaments using CryoSat-2 and Jason-1 satellite-derived gravity data: Evidence of a uniform tectonic activity over the middle part of the Central Indian Ridge. *Physics and Chemistry of the Earth, Parts A/B/C*, 128, <https://doi.org/10.1016/j.pce.2022.103237>
- Salem, A., Williams, S., Fairhead, D., Smith, R., & Ravat, D. (2008). Interpretation of magnetic data using tilt-angle derivatives. *Geophysics*, 73(1), L1-L10. <https://doi.org/10.1190/1.2799992>
- Sampietro, D., & Capponi, M. (2021). Gravity for lithosphere architecture determination and analysis: the Central Eastern Mediterranean case study. *Geophysical Prospecting*, 70(1), 173-192. <https://doi.org/10.1111/1365-2478.13146>
- Simpson, S. M. (1954). Least squares polynomial fitting to gravitational data and density plotting by digital computers. *Geophysics*, 19(2), 255-269. <https://doi.org/10.1190/1.1437990>
- Spector, A., & Grant, F. S. (1970). Statistical models for interpreting aeromagnetic data. *Geophysics*, 35(2), 293-302. <https://doi.org/10.1190/1.1440092>
- Taha, A. I., Al Deep, M., & Mohamed, A. (2021). Investigation of groundwater occurrence using gravity and electrical resistivity methods: A case study from Wadi Sar, Hijaz Mountains, Saudi Arabia. *Arabian Journal of Geosciences*, 14, 1-10. <https://doi.org/10.1007/s12517-021-06628-z>
- Tatchum, C. N., Tabod, T. C., Koumetio, F., & Manguelle-Dicou, E. (2011). A Gravity Model Study for Differentiating Vertical and Dipping Geological Contacts with Application to a Bouguer Gravity Anomaly Over the Fouban Shear Zone, Cameroon. *Geophysica*, 47(1-2), 43-55.
- Thompson, D. T. (1982). EULDPH: A new technique for making computer-assisted depth estimates from magnetic data. *Geophysics*, 47(1), 31-37. <https://doi.org/10.1190/1.1441278>
- Ting-jie, Y. A. N., Yan-Gang, W. U., Yuan, Y. U. A. N., & Ling-Na, C. H. E. N. (2016). Edge detection of potential field data using an enhanced analytic signal tilt angle. *Chinese Journal of Geophysics*, 59(4), 341-349. <https://doi.org/10.1002/cjg2.20239>
- Ugbor, C. C., Emedo, C. O., & Arinze, I. J. (2021). Interpretation of airborne magnetic and geo-electric data: resource potential and basement morphology of the Ikom-Mamfe Embayment and Environs, Southeastern Nigeria. *Natural Resources Research*, 30, 153-174. <https://doi.org/10.1007/s11053-020-09725-0>
- Uieda, L., Barbosa, V. C., & Braitenberg, C. (2016). Tesseroids: Forward-modeling gravitational fields in spherical coordinates. *Geophysics*, 81(5), F41-F48. <https://doi.org/10.1190/geo2015-0204.1>
- Wang, G., & Huang, L. (2012). 3D geological modeling for mineral resource assessment of the Tongshan Cu deposit, Heilongjiang Province, China. *Geoscience Frontiers*, 3(4), 483-491. <https://doi.org/10.1016/j.gsf.2011.12.012>
- Wijns, C., Perez, C., & Kowalczyk, P. (2005). Theta map: Edge detection in magnetic data. *Geophysics*, 70(4), L39-L43. <https://doi.org/10.1190/1.1988184>
- Ziani, S., Khattach, D., Abderbi, J., & Nouayti, N. (2022). Structural modeling of deep aquifers from gravity data: a case study of the Isly watershed, region of Guenfouda, Morocco. *Modeling Earth Systems and Environment*, 8(3), 3757-3767. <https://doi.org/10.1007/s40808-021-01324-z>
- Zingerle, P., Pail, R., Gruber, T., & Oikonomidou, X. (2020). The combined global gravity field model XGM2019e. *Journal of Geodesy*, 94, 1-12. <https://doi.org/10.1007/s00190-020-01398-0>